Nano Research 2015, 8(5): 1563–1576
DOI 10.1007/s12274-014-0642-5
Research Article
ISSN 1998-0124
CN 11-5974/O4

Aggregation-induced emission (AIE) dye loaded polymer nanoparticles for gene silencing in pancreatic cancer and their *in vitro* and *in vivo* biocompatibility evaluation

Rui Hu[1], Chengbin Yang[1], Yucheng Wang[1], Guimiao Lin[2], Wei Qin[3], Qingling Ouyang[1], Wing-Cheung Law[4], Quoc Toan Nguyen[5], Ho Sup Yoon[5], Xiaomei Wang[2], Ken-Tye Yong[1] (✉), and Ben Zhong Tang[3] (✉)

[1] *School of Electrical and Electronic Engineering, Nanyang Technological University, Singapore 639798, Singapore*
[2] *The Engineering Lab of Synthetic Biology and the Key Lab of Biomedical Engineering, School of Medicine, Shenzhen University, Shenzhen 518060, China*
[3] *Department of Chemistry, The Hong Kong University of Science and Technology, Clear Water Bay, Kowloon, Hong Kong, China*
[4] *Department of Industrial and Systems Engineering, The Hong Kong Polytechnic University, Hung Hom, Kowloon, Hong Kong, China*
[5] *Division of Structural Biology & Biochemistry, School of Biological Sciences, Nanyang Technological University, Singapore 639798, Singapore*

Received: 14 August 2014
Revised: 8 November 2014
Accepted: 14 November 2014

KEYWORDS
aggregation-induced emission,
polymer nanoparticles,
gene silencing,
pancreatic cancer

ABSTRACT

We have developed aggregation-induced emission (AIE) dye loaded polymer nanoparticles with deep-red emission for siRNA delivery to pancreatic cancer cells. Two US Food and Drug Administration (FDA) approved surfactant polymers, Pluronics F127 and PEGylated phospholipid, were used to prepare the dye-loaded nanoparticle formulations and they can be used as nanovectors for gene silencing of mutant K-ras in pancreatic cancer cells. The successful transfection of siRNA by the developed nanovectors was confirmed by the fluorescent imaging and quantified through flow cytometry. Quantitative real time polymerase chain reaction (PCR) indicates that the expression of the mutant K-ras oncogene from the MiaPaCa-2 pancreatic cancer cells has been successfully suppressed. More importantly, our *in vivo* toxicity study has revealed that both the nanoparticle formulations are highly biocompatible in BALC/c mice. Overall, our results suggest that the AIE dye-loaded polymer nanoparticle formulations developed here are suitable for gene delivery and have high potential applications in translational medicine research.

1 Introduction

Gene therapy has emerged as a valuable medicinal approach for combating cancers [1, 2]. Among the gene therapy strategies, the RNA interference (RNAi) method has been extensively studied and employed

Address correspondence to Ken-Tye Yong, ktyong@ntu.edu.sg; Ben Zhong Tang, tangbenz@ust.hk

in cancer therapy [3]. This strategy relies on a post-transcriptional gene silencing process that uses a sequence specific double-stranded RNA to initiate the degradation of a targeted messenger RNA (mRNA) homologous. In a typical RNAi process, synthetic small interfering RNAs (siRNAs) are transfected into the cytoplasm and incorporated into a nuclease complex, the RNA-induced silencing complex (RISC), which then binds to the target mRNA and subsequently cause its rapid degradation [4, 5]. As a result, the mRNA translation is interrupted to produce functional proteins. The successful intracellular transfection of siRNAs is dependent on the siRNA carrier system. By nature, "naked" siRNAs are negatively charged and they are susceptible to nuclease-mediated degradation. Thus, a carrier system is needed to deliver them into the cells [6]. It is commonly known that viral vectors are useful carrier systems for gene delivery owing to their high transfection efficiency [1]. However, some studies have discovered that these vectors induced harmful immune responses and displayed high biosafety risks for gene therapy use [7]. More recently, the nanomedicine research community has focused on engineering non-viral nanoparticle based vectors such as magnetic nanoparticles, metallic nanoparticles, quantum dots, carbon based nanoparticles and polymer nanoparticles for safer and more effective gene delivery therapy applications [7]. These nanoparticles have rich surface chemistries, thus allowing one to incorporate additional functions into the particle, such as tracking and imaging, co-delivery of drugs, targeted delivery and photothermal therapy for enhancing the overall therapeutic effects of gene delivery therapy [8–11]. The use of these nanoparticles in gene delivery has laid an important foundation for preparing clinical usable gene transfecting agents in the near future.

Polymer based fluorescent nanoparticles have been extensively used in biomedical research ranging from imaging to drug delivery [12]. These particles can be prepared using simple synthesis protocols and they are highly biocompatible for biological use. More importantly, they are biodegradable and they can be removed from the body after completing their programmed tasks [13]. Typically, polymer-based fluorescent nanoparticles are prepared by loading organic π-conjugated fluorophores into the core of hydrophobic polymer particles. The loading fluorophore concentration is a crucial parameter for determining the overall brightness of the nanoparticle formulation. At relatively low loading concentration, the fluorescence intensity of the nanoparticles is linearly dependent on the dye loading efficiency. However, as the dye concentration increases, the dye molecules start to aggregate in the particle core and this phenomena will lead to quenching of light emission of the dyes [14]. This aggregation caused quenching (ACQ) behavior is mainly resulted from the π–π stacking between the aggregated dye molecules and this has been a major hurdle for preparing polymer-based fluorescent nanoparticles with high loading dye concentration [15]. This obstacle has been overcome by Tang and coworkers using aggregated dyes [16, 17]. In 2001, they demonstrated the process of aggregation-induced emission (AIE) in a silole fluorogen system (1-methyl-1,2,3,4,5-pentaphenyl silole), where the dye molecules become highly emissive in the aggregated form [18]. The key to this phenomenon lies in the chemical structure of the silole molecule where five phenyl peripheries are attached to one silole core through single-bond axes. In the non-aggregated form, the intracellular rotation of the peripheries is not confined which provides a non-radiative relaxation channel for the excited state to decay. However, in the aggregated state, the physical constraint between the dyes prevents the peripheries from rotating and inactivating the non-radiative channel and thus causing the aggregates to emit fluorescence. This restricted intramolecular rotation (RIR) theory has then been used to explain the highly emissive behavior of AIE systems and applied for developments of new AIE fluorogens [19–21]. Recently, we have developed a synthesis method to incorporate conventional ACQ chromophores into AIE fluorogens through covalent integration steps [22]. More importantly, this method can be used to incorporate a wide variety of ACQ chromophores for creating different emission wavelengths while inheriting the AIE feature.

Previously, we have designed and synthesized a TPE–TPA–DCM compound (2-(2,6-bis((E)-4-(phenyl(4′-(1,2,2-triphenyl vinyl)-[1,1′-biphenyl]-4-yl)amino)styryl)-4*H*-pyran-4-ylidene)malononitrile) by conjugating the red emitting ACQ chromophore TPA–DCM (2-(2,6-bis((E)-

4-(diphenylamino)styryl)-4*H*-pyran-4-ylidene)malononitrile) to an AIE luminogen TPE (tetraphenylethene) [23]. The resulting compound preserves the AIE properties and was encapsulated into cross-linked bovine serum albumin (BSA) nanoparticles for *in vitro* and *in vivo* imaging applications. In this contribution, two polymer-based fluorescent nanoparticle formulations were prepared by encapsulating the TPE–TPA–DCM compound with the US Food and Drug Administration (FDA) approved PEGylated phospholipid [24, 25] or tri-block copolymer Pluronic F127 [26, 27] for pancreatic cancer gene therapy. Synthetic siRNA molecules specifically targeting the mutated K-ras gene were complexed to the modified polymer nanoparticle surface through layer-by-layer assembling approach. The K-ras gene is reported to have the highest alteration frequency in pancreatic cancers [28]. This key oncogene has been widely studied by the pancreatic cancer research community since it is associated with a series of downstream genes that regulate tumor cell proliferation, migration and invasion [29–31]. The siRNA-complexed nanoparticles were then used for the transfection of pancreatic cancer cells MiaPaCa-2. The successful delivery of the nanoplexes to the MiaPaCa-2 cells was confirmed through optical imaging study by monitoring the fluorescence from the AIE dye and the FAM-labeled siRNA molecules. Flow cytometry was then used to quantify the transfection efficiency of the siRNA-complexed nanoparticles. Through real-time polymerase chain reaction (PCR) experiments, we have observed that both the formulations were capable of suppressing the K-ras gene expression with efficiency as high as 70%. In addition to gene delivery study, we have also evaluated the *in vitro* and *in vivo* toxicity of the dye-loaded nanoparticle formulations. *In vitro* (3-(4,5-dimethylthiazol-2-yl)-2,5-diphenyltetrazolium bromide) (MTT) assay shows that the phospholipid micelle encapsulated nanoparticle formulation is slightly toxic and a cell viability of 70% was observed at high dosage (2.5 μg·mL^{-1}) after 48 h of treatment. On the other hand, the Pluronic F127 nanoparticles formulation displayed a much better biocompatibility when compared to phospholipid nanoparticle formulation. Even though the nanoparticles promote *in vitro* toxicity at high concentration, they are highly biocompatible *in vivo*. In our *in vivo* study, mice treated with both formulations at a dosage of 1.5 mg·kg^{-1} did not show any adverse response over six weeks of evaluation. No pathological abnormalities were observed from the histological analysis of the major organs obtained from the treated mice. In the near future, we envision that the AIE dye-loaded polymer nanoparticles will become valuable tools for gene delivery therapy *in vivo*.

2 Materials and methods

2.1 Nanoparticle preparation and characterization

The AIE dye TPE–TPA–DCM was synthesized according to our previous method [23]. To fabricate the nanoparticles, mPEG-DSPE-5000 (1,2-diacyl-sn-glycero-3-phosphoethanolamine-*N*-[methoxy(polyethylene glycol)], Laysan Bio Inc.) was mixed with the AIE dye in chloroform in weight ratios of 9:1 and 19:1 in a round bottom flask. The chloroform was then gently removed by a vacuum rotary evaporator with a room temperature water bath. After that, 10 mL of water was added to the lipidic layer and the flask was gently stirred for 20 min. The resulting mixture was then filtered through a 0.2 μm syringe filter to remove large aggregates. This results in phospholipid encapsulated AIE dye nanoparticles with loading ratios of 10% or 5%. A similar procedure was used for the preparation of the Pluronic F127 (BASF Corp., Wyandotte, MI) encapsulated nanoparticles simply by replacing mPEG-DSPE-5000 with Pluronic F127. For siRNA conjugation, the nanoparticles were first coated with a thin layer of PAH (poly(allylamine hydrochloride, Mw = 15 kDa, Sigma-Aldrich) and centrifuged at 15,000 rpm for 30 min. The pellet was then collected for siRNA conjugation through electrostatic absorption. The absorption spectra of the dye nanoparticles were collected using a Shimadzu model UV-2450 spectrophotometer, where corresponding solvents were used as references. The photoluminescence emission spectra were collected by a Fluorolog-3 spectrofluorometer (Edison, NJ USA). To estimate the fluorescent quantum yield (QY) of the nanoparticle formulations, integrated emission spectra of diluted nanoparticle suspensions were compared with rhodamine 6G. The absorptions were matched at the excitation wavelength

of 500 nm. The hydrodynamic size distribution and zeta potential of the nanoparticles were measured using the 90Plus particle analyzer (Brookhaven Instruments). All measurements were carried out at room temperature.

2.2 Cell culture and viability studies

MiaPaCa-2 (ATCC NO: CRL-1420) cells were maintained in Dulbecco's modified Eagle's medium (DMEM, Life Technologies) supplemented with 10% fetal bovine serum (FBS). The cells were cultured at 37 ˚C in a humidified atmosphere with 5% CO_2. Cell viability was measured by the MTT (Sigma) assay kit as previously described [32]. Briefly, in each assay, 5,000 cells were dispensed into each well of a 96-well flat-bottom Microtiter plate and cultured overnight. Eight sets were treated with different concentrations of nanoparticle formulations and one set was treated with PBS buffer as the non-treated control. The cells were subsequently incubated for 24 h or 48 h before the assay. To perform the assay, 20 μL of MTT reagent was added to each well and incubated for another four hours. 150 μL of dimethylsulfoxide (DMSO, Sigma) was then added to dissolve the precipitate with 5 min gentle shaking. Absorbance was then measured with a microplate reader (Bio-Rad) at the wavelength of 490 nm. The cell viability was obtained by normalizing the absorbance of the sample against the control well and expressed as percentage, assigning the viability of non-treated cells as 100%. Assays were performed in triplicate and the results were averaged.

2.3 Transfection, flow cytometry measurement and cell imaging

MiaPaCa-2 cells (1×10^4) were seeded onto six-well plates in DMEM medium without antibiotics to give 30–50% confluence at the time of transfections. Phos-10% and F127-10% nanoparticles were mixed with 20 μL of 10 μM K-ras siRNA (Sense: 5′-FAM-GUUGGAGCU***UGU***GGCGUAGUU-3; Antisense: 5-CUACGCCACAAGCUCCAACUU-3,) with gentle vortex and incubated for 20 minutes. Before transfection, the culture medium was replaced with FBS-free DMEM medium, the above mentioned nanoparticle-siRNA nanoplex formulations were then added to the six-well plate wells and the cells were continuously cultured. For flow cytometry analysis, cells were digested by trypsin after 24 hours of transfection and washed twice with phosphate-buffered saline (PBS). Samples were analyzed using a FACSCalibur flow cytometer (Becton Dickinson, Mississauga, CA). *In vitro* fluorescence microscopy images were obtained using fluorescence microscope (Eclipse-Ti, Nikon) with appropriate fluorescent filter cubes. After 4 h of incubation, the nanoplex transfected cells were washed twice with PBS, and fixed with 4% formaldehyde. The cell nuclei were stained with 4',6-diamidino-2-phenylindole (DAPI) (Sigma). For both flow cytometry analysis and fluorescent imaging, siRNAs were labeled with fluorescent FAM.

2.4 Gene expression analysis

Forty-eight hours after transfection, total RNA was extracted from MiaPaCa-2 cells using a E.Z.N.AtM Total RNA Kit (OMEGA) and the amount was quantitated by a spectrophotometer (Nano-Drop ND-1000). Reverse transcription was conducted in a 20 μL reaction mixture and cDNA was synthesized from 2 μg of total RNA using the reverse transcriptase kit (Promega) according to the previous experience [33]. The K-ras relative mRNA expression level was determined using quantitative real time qRT-PCR normalized to the expression of β-Actin, one of the most commonly used housekeeping genes adopted in comparisons of gene expression [34]. According to the previous report [35], the primer sequences for different genes were as follows: K-ras, forwards 5′-AGAGTGCCTTGACGATACAGC-3′ and reverse 5′-ACAAAGAAAGCCCTCCCCAGT-3′; β-Actin, forwards 5'-CGGAACCGCTCATTGCC-3′ and reverse 5'-ACCCACACTGTGCCCATCTA-3′.

2.5 Animal maintenance and pathological study

BALB/C mice were obtained from the Medical Laboratory Animal Center of Guangdong Province and handled with protocols approved by the Laboratory Animals Center of Shenzhen University. All the animal experiments and maintenance were approved by the Experimental Animal Ethics Committee of Shenzhen University. BALB/C mice were obtained at 8 weeks of age and were housed 5 per cage in a 12 h/12 h

light/dark cycle. All animals were fed with water and standard laboratory chow ad libitum. The mice were injected with 200 μL of buffer saline or buffered nanoparticle dispersions. At different periods after injection the mice were weighed and evaluated for behavioral changes. For pathological analysis, the animals were sacrificed after 42 days of treatment. The major organs (heart, liver, spleen, lung, kidney and brain) of the mice were harvested and embedded in paraffin, sectioned, and stained with hematoxylin and eosin (H&E staining). The H&E staining slices were examined under an optical microscope (Olympus BX51) by a clinical pathologist.

3 Results and discussion

In our study, two different polymer materials, namely PEGylated phospholipid and Pluronic F127, were used to encapsulate the AIE dye and create the polymer-based fluorescent nanoparticles. The encapsulation process is straightforward and the steps are schematically illustrated in Fig. 1. Two different loading ratios of 10% and 5% of AIE dye molecules were used to synthesize dye-loaded nanoparticles and this strategy has allowed us to generate four types of nanoparticle formulations which are referred as Phos-10%, Phos-5%, F127-10% and F127-5%. Figure 2 shows the extinction and photoluminescence (PL) spectra of the different types of nanoparticle formulations. Similar extinction spectra features were observed for both AIE dye-loaded nanoparticles dispersion and "free" dyes in chloroform solution. However, this is not the case for the PL spectra. The emission peak of the AIE dyes red-shifted from 620 to 660 nm after they were loaded into polymer nanoparticles and this indicates that the AIE dyes are aggregated in the particle cores. This observation is consistent with previous reports. The fluorescent quantum yields (QY) of the encapsulated nanoparticles were estimated to be around 6.4% and 12.6% for Phos-5% and Phos-10% formulations, respectively. Similar QY values of 6.7% and 12.9% for F127-5% and F127-10% were also observed. Figure 3 shows the hydrodynamic size distribution of the prepared nanoparticles. It has been reported that the aggregation number of micelles is affected by several factors such as the amphiphile

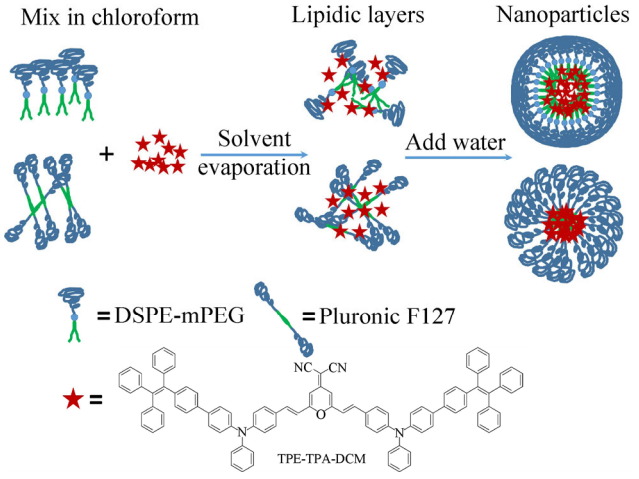

Figure 1 Schematic illustration of the construction of nanoparticle formulations based on PEGylated phospholipid and triblock co-polymer Pluronic F127.

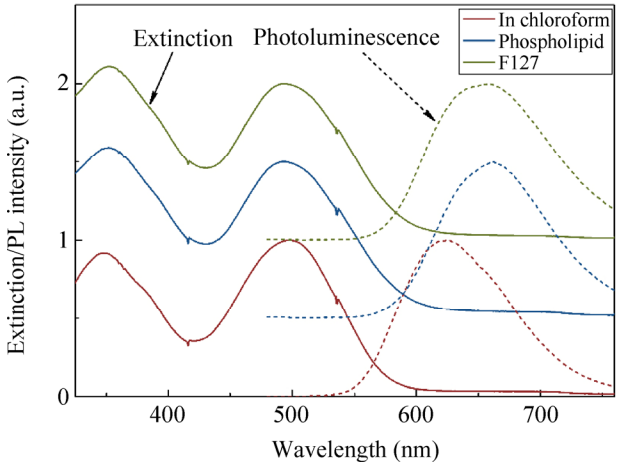

Figure 2 Extinction and photoluminescence spectra of the AIE dye in chloroform and encapsulated in polymer nanoparticles.

material itself, temperature, counterion radius and ionic strength [36, 37]. In our case, the phospholipid micelle encapsulated AIE dye nanoparticles have a larger hydrodynamic diameter size when compared to Pluronic F127 encapsulated AIE dye nanoparticles. It is worth noting that the phospholipid micelle encapsulated AIE dye nanoparticle size is dependent on the dye concentration loaded within the particle. As organic additives generally decrease the aggregation number of a micellar system [36], this could explain why the average hydrodynamic particle size for the Phos-10% (165.2 nm) is smaller than the Phos-5% formulation (190.4 nm). On the other hand, although the aggregation pattern of the triblock co-polymer Pluronic F127 is very different from that of the

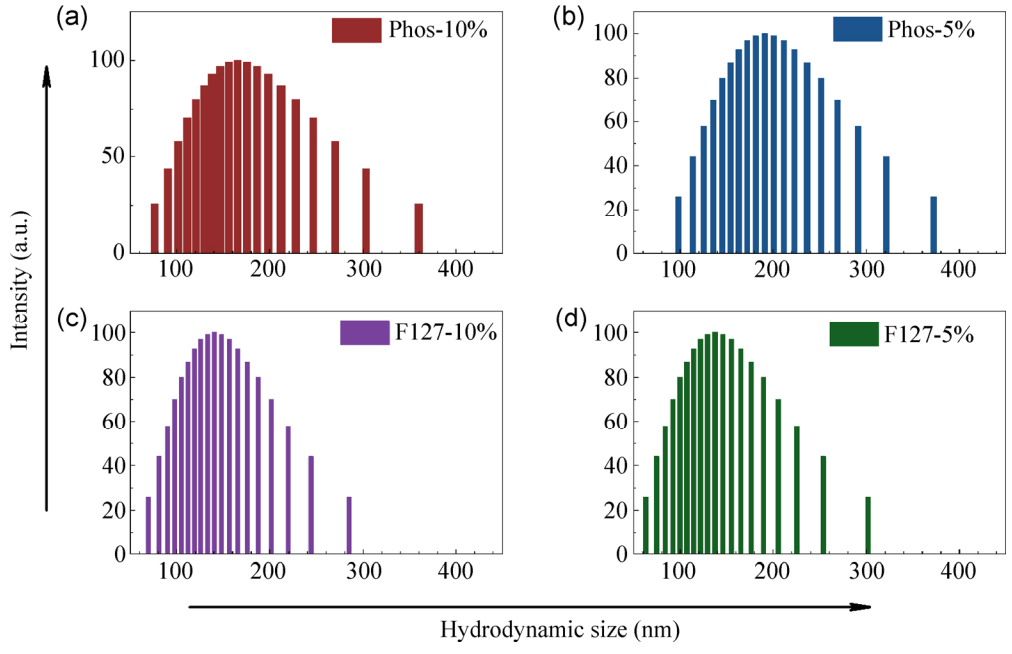

Figure 3 Hydrodynamic size distribution of different AIE dye encapsulated formulations. (a) Phos-10%, PEGylated phospholipid encapsulated AIE dye nanoparticles with a feeding ratio of 10 wt.%. (b) Phos-5%, PEGylated phospholipid encapsulated AIE dye nanoparticles with a feeding ratio of 5 wt.% (c) F127-10%, Pluronic F127 encapsulated AIE dye nanoparticle with a feeding ratio of 10 wt.%. (d) F127-5%, Pluronic F127 encapsulated AIE dye nanoparticles with a feeding ratio of 5 wt.%.

phospholipid micellar system [38–41], we observed that the loaded dye concentration did not affect the average size of the nanoparticles. The measured sizes were 140.3 nm and 137.5 nm for F127-10% and F127-5%, respectively.

Prior to embarking on the gene delivery study, the cytotoxicity of the prepared nanoparticle formulations was examined by using cell viability assay. As shown in Fig. 4, the cell viability of MiaPaCa-2 cells remained around 80% after treatment with the prepared formulations at different dosages. The result shows that both the phospholipid micelle and the Pluronic F127 encapsulated AIE dye nanoparticle formulations have relatively high biocompatibility within the tested dosage range in this experiment. However, we did notice that the cells treated with the phospholipid micelle encapsulated dye nanoparticle formulation have a slightly lower viability compared to the cells treated with the Pluronic F127 micelle-encapsulated dye particle formulation. This may be due to the release of the AIE dye molecules from the micelle particles or/and the toxicity of the micelle particles.

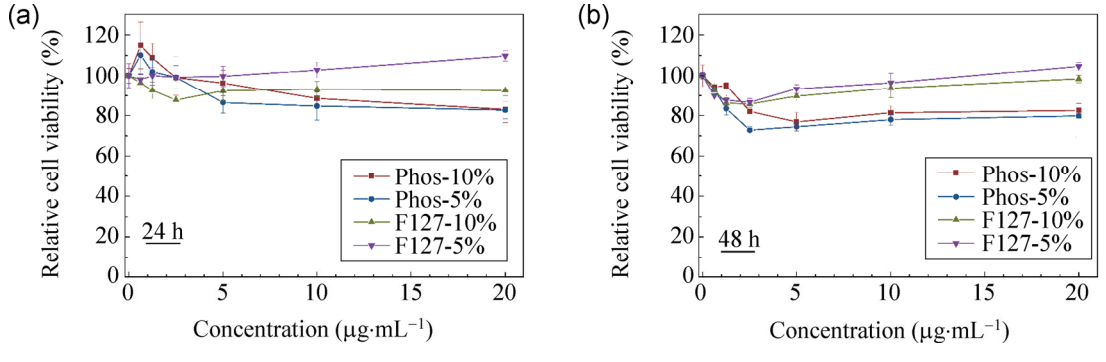

Figure 4 Relative cell viabilities of MiaPaCa-2 cells treated with different concentrations of the four nanoparticle formulations, after 24 h (a) or 48 h (b) of treatment.

As reported by Wang et al., the release rate of dyes from micelle particles becomes higher as the concentration of the loaded dye increases [42], and the free dye becomes a major source of the toxicity in the biological system. The other toxicity source is the PEGylated phospholipid micelle particles themselves. Wang et al. have shown that PEGylated phospholipid micelles can induce endoplasmic reticulum-dependent apoptosis of cancer cells [43]. They found that the PEGylated phospholipid micelle particles were accumulated in the endoplasmic reticulum (ER) and disturb the ER lipid homeostasis, thus causing ER stress to the cancer cells. Under such stress, the cancer cells initiate proapoptotic signaling and undergo ER membrane damage which in turn triggers the caspase-dependent apoptosis process. It is worth mentioning that during the nanoparticle preparation process, chloroform was introduced; this is classified as a group 2B carcinogen by the International Agency for Research on Cancer (IARC) [44]. However, as the cytotoxicity effects of chloroform are reported to be observed at a relatively high concentration of above 4 mM in female rat hepatocytes [45], the trace amount of chloroform in this study was not the main contributing factor to the differences in the cell viabilities between the Pluronic F127 and phospholipid formulations.

To conjugate siRNAs for intracellular gene delivery, it is required that the nanoparticles have a positively charged surface. The prepared micelle-encapsulated AIE dye nanoparticles in this study are negatively charged due to the PEGylated surface of the particles. To reverse the surface charge of the particles, a positively charged polyelectrolyte poly(allylamine hydrochloride) (PAH) was added to the nanoparticle surface through a layer-by-layer assembly process. Figure 5 shows the zeta potential of the four nanoparticle formulations before and after PAH modification. The charge reversal from negative to positive clearly reveals the successful coating of PAH on the nanoparticle surface. As a demonstration, the two formulations with higher dye doping ratios, Phos-10% and F127-10%, were used as nanocarriers for siRNA delivery studies. SiRNAs targeting the mutant K-ras gene of MiaPaCa-2 cells were complexed to the micelle-encapsulated AIE dye nanoparticles through electrostatic interaction. These two nanoplex

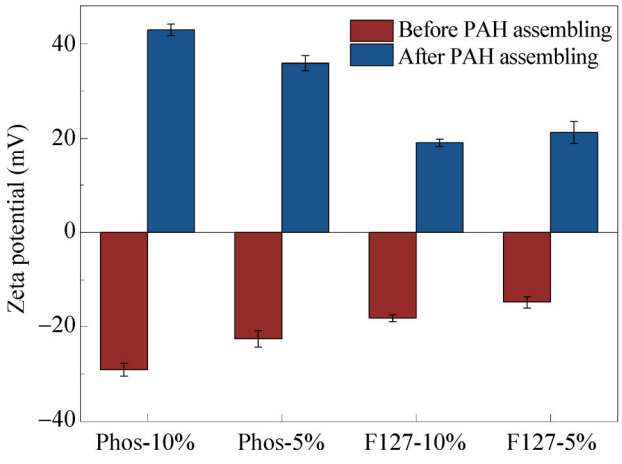

Figure 5 Zeta potential values of the four formulations before and after PAH assembling

formulations, referred as Phos-10%-siRNA and F127-10%-siRNA, were used for transfection of MiaPaCa-2 cells. Figure 6 shows the fluorescent images of cells treated with Phos-10%-siRNA and F127-10%-siRNA nanoformulations, where the siRNAs were labeled with a fluorescent tag FAM for monitoring the biodistribution of the nanoparticles. From the fluorescent images, one can observe that both formulations have successfully delivered siRNAs into the cancer cells, and this is confirmed by the co-localization of the red (AIE dye) and green ($siRNA^{FAM}$) fluorescent signals around the cell nucleus. In contrast, no green signals were detected from cells treated with free siRNAs (data not shown). The endosomal escape and siRNA release from the nanocarriers are the two key steps that siRNA-based RNAi needs to carry out efficiently. Several mechanisms have been reported to be responsible for the endosomal escape, such as the pore formation in the endosomal membrane, pH-buffering effect, endosomal membrane fusion and photochemical disruption of the endosomal membrane [46, 47]. For example, some viruses tend to escape through a fusion process, where conformational changes of fusogenic peptides are involved in inducing the fusion in the lipid bilayers of the endosomes [48, 49]. Similarly, the cationic liposomes are able to escape from the endosomes based on this pathway [50]. They usually introduce a neutral helper lipid, such as dioleoylphosphatidylethanolamine (DOPE), to enhance the fusion between the liposomes and the endosomal membrane [51, 52]. The pH-buffering effect, also known as the proton sponge effect,

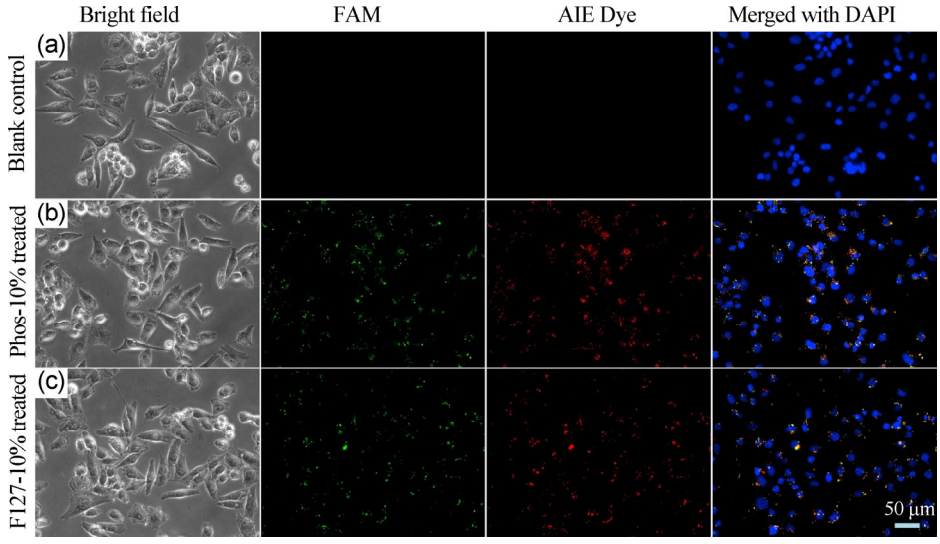

Figure 6 Fluorescent imaging of MiaPaCa-2 cells treated with AIE dye doped nanoparticle formulations. (a) Blank control, (b) Phos-10% and (c) F127-10%. The FAM labeled siRNAs and AIE dye were rendered in green and red, respectively. Cell nuclei are stained with DAPI and rendered in blue.

is another endosomal escape mechanism which is commonly adopted in designing the transfection agent to assist the payload release [53]. In such process, a positively charged polymer—such as polyethylenimine [54] or poly(amidoamine) [55]—or methylamine [56], is usually used to modify the surface of the transfection agent, in order to induce the extensive inflow of ions and water into the endosomal environment to break the endosomal membrane, thus setting free the substances encapsulated within the particle. The PAH used in this study is a positively charged polymer with an abundance of primary amine groups. Based on these facts, formulation takes place, the PAH causes the inflow of ions into the endosomes, and subsequently induces the endosomal escape of the nanoplexes through proton sponge effects. From the fluorescence images, we can clearly identify the red and green signals. Since naked siRNAs cannot enter the cells without any transfection agents, this indicates that the siRNA molecules have detached from the nanoplex particles and gradually diffused into the local cytoplasm environment to initiate the RNAi process.

To quantify the siRNA transfection efficiency of the nanoparticle formulations, flow cytometry analysis was performed. In this experiment, a reference gate (Fig. 7(a)) was used to exclude the cell debris and the fluorescent dot-plots were divided into four different zones using the blank control as reference (Figs. 7(b)–7(d)). As shown in Fig. 7(c), most of the Phos-10%-siRNA treated cells displayed red fluorescence originating from the AIE dye, and the fluorescence from the FAM label is relatively weak. In comparison, the cells treated with F127-10%-siRNA have strong fluorescent signals from the FAM label (Fig. 7(d)). The statistical results of the flow cytometry analysis are summarized in Fig. 7(e). The transfection efficiency is defined as the population of FAM-positive cell counts and the labeling efficiency is defined as the cell counts displayed by fluorescence from the AIE dye. Our results show that both the phospholipid and Pluronic F127 micelle-encapsulated AIE dye nanoparticle formulations are able to serve as nanocarriers for transfecting the cells with siRNAs molecules. The Phos-10%-siRNA formulation has a relatively high labeling efficiency when compared to the F127-10%-siRNA formulation. However, it possesses relatively lower transfection efficiency (41.3 ± 0.26%) when compared to the F127-10%-siRNA formulation (78.5 ± 0.21%). As the two particle formulations have different aggregation patterns, the kinetic release rates of siRNAs from the nanoplexes are different from one another. It was reported that a burst release of 20–30% siRNA was observed in the first 24 hours in an *in vitro* study involving the use of a polyethylenimine (PEI) modified PLGA nanoparticle formulation [57]. In addition, the fusion of phospholipid

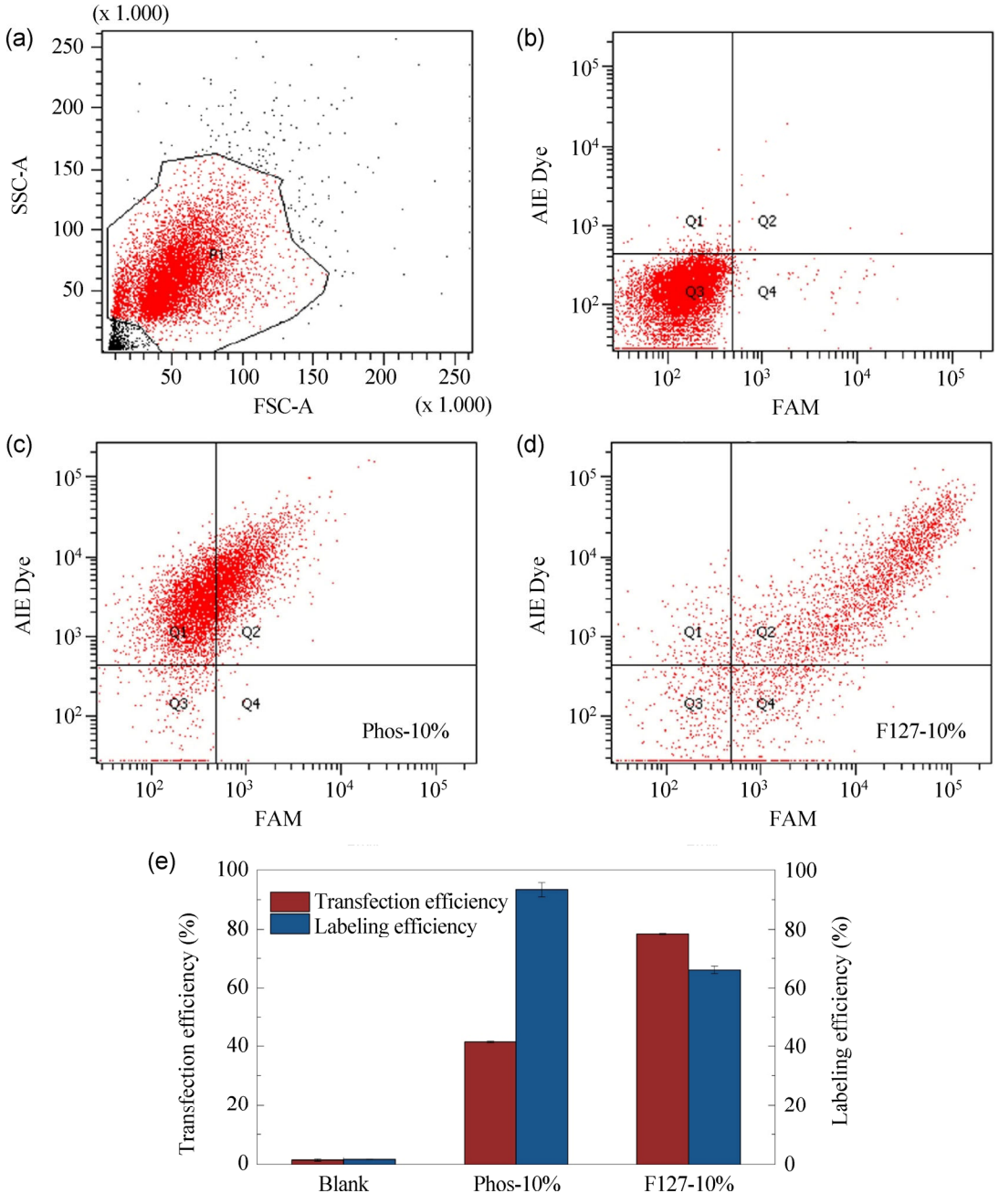

Figure 7 Flow cytometry analysis of MiaPaCa-2 cells transfected with Phos-10% and F127-10% formulations. (a) Reference gate definition. Dot plots of cells treated with saline (b), Phos-10% (c) and F127-10% (d). (e) Statistical evaluation of the dot plots showing the transfection and labeling efficiency.

molecules with the endosomal membrane accelerated the disruption of the particle and subsequent release of siRNA molecules [58, 59]. These two key factors may have contributed to the low transfection efficiency of the Phos-10%-siRNA formulation. To investigate the gene silencing efficiency of the nanoplexes, the K-ras mRNAs expression of the cells was measured by quantitative real time PCR. As shown in Fig. 8, both the Phos-10% and F127-10% nanoformulations showed effective knockdown of the mutant K-ras gene, with efficiencies of 83.52 ± 2.45% and 74.96 ± 1.41%, respectively. The down regulation of gene expression confirms the successful siRNA transfection by the nanoparticle formulations. This indicates that the

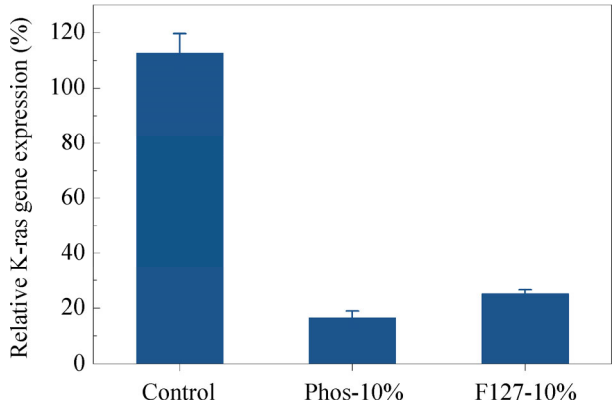

Figure 8 K-Ras mRNA relative expression levels detected by quantitative real time RT-PCR in MiaPaCa-2 cells treated with Phos-10% or F127-10% formulation, as compared with non-treated control.

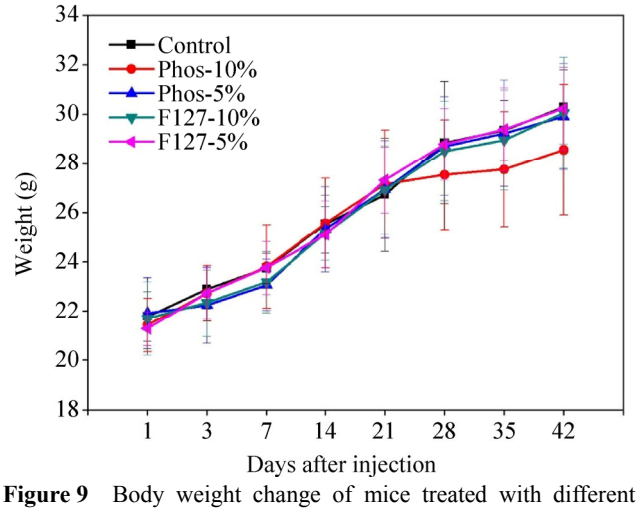

Figure 9 Body weight change of mice treated with different nanoparticle formulations.

siRNAs are delivered into the cells and released in the cytoplasm, and then subsequently bind to the targeting mRNA thus initiating the gene silencing process. To date, many mutations in pancreatic cancer have been found in human genes [60], such as HER2/neu [61], p16INK4 [62], p53 [63] and BRCA2 [64], but K-ras oncogene has been identified as having the highest alteration frequency and it usually starts to develop in the early stages of pancreatic cancer [65, 66]. More importantly, the mutation of K-ras oncogene is associated with a series of downstream gene regulation that is related to the proliferation, migration and invasion of pancreatic cancer cells [67, 68]. *In vitro* studies have found that silencing of the mutant K-ras in pancreatic cancer through RNAi methods promotes cell apoptosis [69–72], and inhibit cell proliferation [73, 74], migration [75] and invasion of the tumor cells [76]. Thus, the use of micelle-encapsulated AIE dye nanoparticles for down regulating the K-ras gene expression of pancreatic cancer will be a useful approach in the near future for effective therapy of pancreatic cancer *in vivo*.

In addition to an *in vitro* study, we also tested the *in vivo* biocompatibility of our prepared nanoformulations. In this experiment, all of the four polymer-encapsulated AIE dye nanoparticle formulations—Phos-10%, Phos-5%, F127-10% and F127-5%—were intravenously administered to BALB/C mice at a relatively high dosage of 1.5 mg·kg^{-1}. The treated mice were monitored for over six weeks and no significant changes in body weight were observed in the experimental groups when compared to the control group that received only buffer solution (Fig. 9). Also, histological analysis was performed on the tissue sections obtained from the major organs of the mice after six weeks of nanoparticle treatment (Fig. 10). All the tissue sections including the heart, liver, lung, spleen, kidney and brain were carefully evaluated by a pathologist. Normal hepatocytes were observed in the liver sections and no inflammatory response was identified. Red pulp and white pulp structure features were clearly observed in the spleen tissue section and no infiltration of granulocytes was detected. No pulmonary fibrosis was found in the lung tissue sections and normal glomerulus structures were observed in the kidney tissue sections. No necrosis was observed in all the examined tissue sections. This indicates that both the nanoparticle formulations employed here have the potential to be translated for clinical research testing of pancreatic cancer gene therapy using higher hierarchy animal subjects.

4 Conclusions

We have synthesized polymer micelle-encapsulated AIE dyes nanoparticles as nanocarriers for siRNA delivery in pancreatic cancer cells. The AIE dye was synthesized by covalently conjugating the ACQ chromophore TPA–DCM to an AIE luminogen TPE. The resulting TPE–TPA–DCM dye preserves the AIE property and shows a strong aggregation-induced fluorescence when encapsulated in either the phospholipid micelle or Pluronic F127 nanoparticle

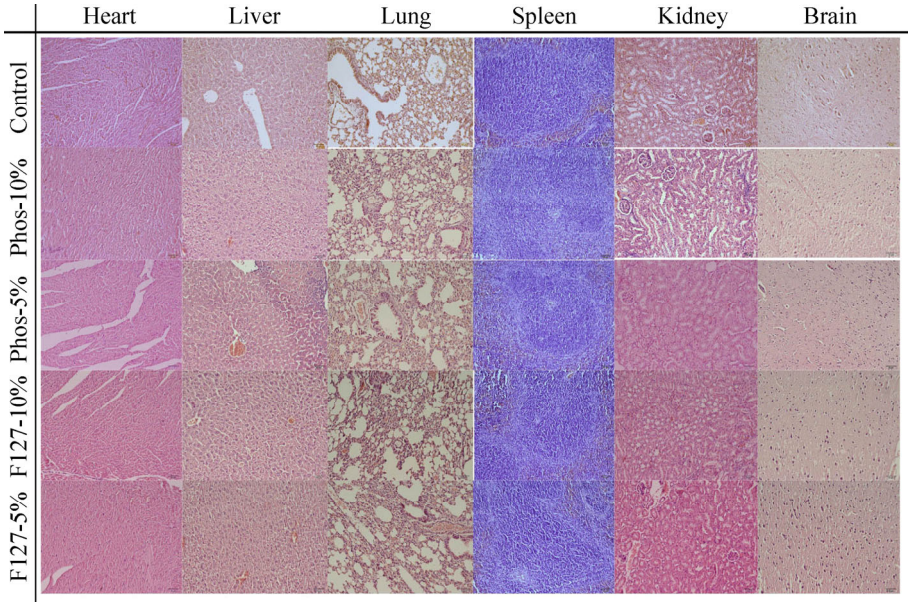

Figure 10 Histological analysis of major organs, including heart, liver, lung, spleen kidney and brain, of mice treated with different nanoparticle formulations of Phos-10%, Phos-5%, F127-10% and F127-5%. No pathological abnormalities were identified in the major organs of the nanoparticle treated animals when compared with the control animals receiving saline solution. All major organs were harvested 6 weeks post injection.

formulations. The prepared nanoparticle formulations were then complexed with siRNAs through layer-by-layer assembly for gene delivery therapy of pancreatic cancer cells. Our results show that the siRNAs can be successfully transfected into the MiaPaCa-2 cells and initiate the RNAi process by using the prepared nanoparticle formulations as the transfection agents. Fluorescence imaging and flow cytometry were used to confirm the successful transfection of siRNA. Quantitative real time PCR indicated the substantial knockdown of the targeted mutant K-ras gene at the mRNA level. In addition, we have evaluated the *in vivo* toxicity of the nanoparticle formulations using BALB/c mice. For a six-week experimental period, mice treated with all four nanoparticle formulations at a dosage of 1.5 $mg \cdot kg^{-1}$ did not show any adverse response. Histological analysis of the major organs obtained from the treated mice did not reveal any observable toxicity effects caused by the dye-loaded nanoparticle formulations. Overall, the dye-loaded nanoparticle formulations prepared in this study have shown promising result for pancreatic cancer gene therapy *in vitro* and we envision that these nanoformulations can be employed in clinical research applications by further optimizing the surface properties of the particle (e.g. by conjugating with ligands for targeted delivery).

Acknowledgement

This work was supported by the National Natural Science Foundation of China (NSFC) (61107017, 81301318), the Start-up grant (M4080141.040) from Nanyang Technological University, Tier 1 Academic Research Funds (M4010360.040 RG29/10) from Singapore Ministry of Education and partially from the Singapore Ministry of Education under a Tier 2 Research Grant MOE2010-T2-2-010 (4020020.040 ARC2/11) and the grant from the Shenzhen Basic Research Project (JC201005280391A)

References

[1] Ginn S. L.; Alexander, I. E.; Edelstein, M. L.; Abedi, M. R.; Wixon, J. Gene therapy clinical trials worldwide to 2012—an update. *J. Gene Med.* **2013**, *15*, 65–77.

[2] Sheridan C. Gene therapy finds its niche. *Nat. Biotechnol.* **2011**, *29*, 121–128.

[3] Peer D.; Lieberman J. Special delivery: targeted therapy with small RNAs. *Gene Ther.* **2011**, *18*, 1127–1133.

[4] Agrawal N.; Dasaradhi P. V. N.; Mohmmed A.; Malhotra P.;

Bhatnagar R. K.; Mukherjee S. K. RNA Interference: Biology, Mechanism, and Applications. *Microbiol. Mol. Biol. R.* **2003**, *67*, 657–685.

[5] Nykänen A.; Haley B.; Zamore P. D. ATP requirements and small interfering RNA structure in the RNA interference pathway. *Cell* **2001**, *107*, 309–321.

[6] Wang J.; Lu Z.; Wientjes M. G.; Au J. L.-S. Delivery of siRNA therapeutics: Barriers and carriers. *AAPS J.* **2010**, *12*, 492–503.

[7] Yin H.; Kanasty R. L.; Eltoukhy A. A.; Vegas A. J.; Dorkin J. R.; Anderson D. G. Non-viral vectors for gene-based therapy. *Nat. Rev. Genet.* **2014**, *15*, 541–555.

[8] Medarova Z.; Pham W.; Farrar C.; Petkova V.; Moore A. *In vivo* imaging of siRNA delivery and silencing in tumors. *Nat. Med.* **2007**, *13*, 372–377.

[9] Lee J. H.; Lee K.; Moon S. H.; Lee Y.; Park T. G.; Cheon J. All-in-One Target-Cell-Specific Magnetic Nanoparticles for Simultaneous Molecular Imaging and siRNA Delivery. *Angew. Chem. Int. Ed.* **2009**, *121*, 4238–4243.

[10] Meng H.; Liong M.; Xia T.; Li Z.; Ji Z.; Zink J. I.; Nel A. E. Engineered design of mesoporous silica nanoparticles to deliver doxorubicin and P-glycoprotein siRNA to overcome drug resistance in a cancer cell line. *ACS Nano* **2010**, *4*, 4539–4550.

[11] Everts M.; Saini V.; Leddon J. L.; Kok R. J.; Stoff-Khalili M.; Preuss M. A.; Millican C. L.; Perkins G.; Brown J. M.; Bagaria H. Covalently linked Au nanoparticles to a viral vector: potential for combined photothermal and gene cancer therapy. *Nano Lett.* **2006**, *6*, 587–591.

[12] Nasongkla N.; Bey E.; Ren J.; Ai H.; Khemtong C.; Guthi J. S.; Chin S.-F.; Sherry A. D.; Boothman D. A.; Gao J. Multifunctional polymeric micelles as cancer-targeted, MRI-ultrasensitive drug delivery systems. *Nano Lett.* **2006**, *6*, 2427–2430.

[13] Farokhzad O. C.; Langer R. Impact of Nanotechnology on Drug Delivery. *ACS Nano* **2009**, *3*, 16–20.

[14] Chen R. F.; Knutson J. R. Mechanism of fluorescence concentration quenching of carboxyfluorescein in liposomes: Energy transfer to nonfluorescent dimers. *Anal. Biochem.* **1988**, *172*, 61–77.

[15] Shirai K.; Matsuoka M.; Fukunishi K. Fluorescence quenching by intermolecular π–π interactions of 2,5-bis(*N*,*N*-dialkylamino)-3,6-dicyanopyrazines. *Dyes Pigm.* **1999**, *42*, 95–101.

[16] Hong Y.; Lam J. W.; Tang B. Z. Aggregation-induced emission: phenomenon, mechanism and applications. *Chem. Commun.* **2009**, 4332–4353.

[17] Hong Y.; Lam J. W. Y.; Tang B. Z. Aggregation-induced emission. *Chem. Soc. Rev.* **2011**, *40*, 5361–5388.

[18] Luo J.; Xie Z.; Lam J. W. Y.; Cheng L.; Chen H.; Qiu C.; Kwok H. S.; Zhan X.; Liu Y.; Zhu D.; Tang B. Z. Aggregation-induced emission of 1-methyl-1,2,3,4,5-pentaphenylsilole. *Chem. Commun.* **2001**, 1740–1741.

[19] Wang Z.; Chen S.; Lam J. W. Y.; Qin W.; Kwok R. T. K.; Xie N.; Hu Q.; Tang B. Z. Long-Term Fluorescent Cellular Tracing by the Aggregates of AIE Bioconjugates. *J. Am. Chem. Soc.* **2013**, *135*, 8238–8245.

[20] Tseng N.-W.; Liu J.; Ng J. C. Y.; Lam J. W. Y.; Sung H. H. Y.; Williams I. D.; Tang B. Z. Deciphering mechanism of aggregation-induced emission (AIE): Is *E–Z* isomerisation involved in an AIE process *Chem. Sci.* **2012**, *3*, 493–497.

[21] Wang P.; Yan X.; Huang F. Host-guest complexation induced emission: a pillar[6]arene-based complex with intense fluorescence in dilute solution. *Chem. Commun.* **2014**, *50*, 5017–5019.

[22] Ding D.; Li K.; Liu B.; Tang B. Z. Bioprobes Based on AIE Fluorogens. *Acc. Chem. Res.* **2013**, *46*, 2441–2453.

[23] Qin W.; Ding D.; Liu J.; Yuan W. Z.; Hu Y.; Liu B.; Tang B. Z. Biocompatible Nanoparticles with Aggregation-Induced Emission Characteristics as Far-Red/Near-Infrared Fluorescent Bioprobes for *In Vitro* and *In Vivo* Imaging Applications. *Adv. Funct. Mater.* **2012**, *22*, 771–779.

[24] Pai A. S.; Rubinstein I.; Önyüksel H. PEGylated phospholipid nanomicelles interact with β-amyloid(1–42) and mitigate its β-sheet formation, aggregation and neurotoxicity *in vitro*. *Peptides* **2006**, *27*, 2858–2866.

[25] Jokerst J. V.; Lobovkina T.; Zare R. N.; Gambhir S. S. Nanoparticle PEGylation for imaging and therapy. *Nanomedicine—UK* **2011**, *6*, 715–728.

[26] Shishido S. l. M.; Seabra A. B.; Loh W.; Ganzarolli de Oliveira M. Thermal and photochemical nitric oxide release from *S*-nitrosothiols incorporated in Pluronic F127 gel: potential uses for local and controlled nitric oxide release. *Biomaterials* **2003**, *24*, 3543–3553.

[27] Liaw J.; Lin Y.-C. Evaluation of poly (ethylene oxide)–poly (propylene oxide)–poly (ethylene oxide) (PEO–PPO–PEO) gels as a release vehicle for percutaneous fentanyl. *J. Control. Release* **2000**, *68*, 273–282.

[28] Smit V. T.; Boot A. J.; Smits A. M.; Fleuren G. J.; Cornelisse C. J.; Bos J. L. KRAS codon 12 mutations occur very frequently in pancreatic adenocarcinomas. *Nucleic Acids Res.* **1988**, *16*, 7773–7782.

[29] Haigis K. M.; Kendall K. R.; Wang Y.; Cheung A.; Haigis M. C.; Glickman J. N.; Niwa-Kawakita M.; Sweet-Cordero A.; Sebolt-Leopold J.; Shannon K. M. Differential effects of oncogenic K-Ras and N-Ras on proliferation, differentiation and tumor progression in the colon. *Nat. Genet.* **2008**, *40*, 600–608.

[30] Campbell P. M.; Groehler A. L.; Lee K. M.; Ouellette M. M.; Khazak V.; Der C. J. K-Ras promotes growth transformation and invasion of immortalized human pancreatic cells by Raf and phosphatidylinositol 3-kinase signaling. *Cancer Res.* **2007**, *67*, 2098–2106.

[31] Dreissigacker U.; Mueller M. S.; Unger M.; Siegert P.; Genze F.; Gierschik P.; Giehl K. Oncogenic K-Ras down-regulates Rac1 and RhoA activity and enhances migration and invasion of pancreatic carcinoma cells through activation of p38. *Cell. Signal.* **2006**, *18*, 1156–1168.

[32] Lin G.; Yang C.; Hu R.; Chen C.-K.; Law W.-C.; Anderson T.; Zhang B.; Nguyen Q. T.; Toh H. T.; Yoon H. S.; Cheng C.; Yong K.-T. Interleukin-8 gene silencing on pancreatic cancer cells using biodegradable polymer nanoplexes. *Biomater. Sci.* **2014**, *2*, 1007–1015.

[33] Yang C.; Mo X.; Lv J.; Liu X.; Yuan M.; Dong M.; Li L.; Luo X.; Fan X.; Jin Z. Lipopolysaccharide enhances FcεRI-mediated mast cell degranulation by increasing Ca^{2+} entry through store-operated Ca^{2+} channels: implications for lipopolysaccharide exacerbating allergic asthma. *Exp. Physiol.* **2012**, *97*, 1315–1327.

[34] Thellin O.; Zorzi W.; Lakaye B.; De Borman B.; Coumans B.; Hennen G.; Grisar T.; Igout A.; Heinen E. Housekeeping genes as internal standards: use and limits. *J. Biotechnol.* **1999**, *75*, 291–295.

[35] Lin G.; Hu R.; Law W.-C.; Chen C.-K.; Wang Y.; Li Chin H.; Nguyen Q. T.; Lai C. K.; Yoon H. S.; Wang X.; Xu G.; Ye L.; Cheng C.; Yong K.-T. Biodegradable Nanocapsules as siRNA Carriers for Mutant K-Ras Gene Silencing of Human Pancreatic Carcinoma Cells. *Small* **2013**, *9*, 2757–2763.

[36] Menger F. M. The structure of micelles. *Acc. Chem. Res.* **1979**, *12*, 111-117.

[37] Benrraou M.; Bales B. L.; Zana R. Effect of the nature of the counterion on the properties of anionic surfactants. 1. Cmc, ionization degree at the cmc and aggregation number of micelles of sodium, cesium, tetramethylammonium, tetraethylammonium, tetrapropylammonium, and tetrabutylammonium dodecyl sulfates. *J Phys. Chem. B* **2003**, *107*, 13432–13440.

[38] Balsara N. P.; Tirrell M.; Lodge T. P. Micelle formation of BAB triblock copolymers in solvents that preferentially dissolve the A block. *Macromolecules* **1991**, *24*, 1975–1986.

[39] Chu B. Structure and dynamics of block copolymer colloids. *Langmuir* **1995**, *11*, 414–421.

[40] Smart T.; Lomas H.; Massignani M.; Flores-Merino M. V.; Perez L. R.; Battaglia G. Block copolymer nanostructures. *Nano Today* **2008**, *3*, 38–46.

[41] Wendoloski J.; Kimatian S.; Schutt C.; Salemme F. Molecular dynamics simulation of a phospholipid micelle. *Science* **1989**, *243*, 636–638.

[42] Wang D.; Qian J.; Qin W.; Qin A.; Tang B. Z.; He S. Biocompatible and Photostable AIE Dots with Red Emission for *In vivo* Two-Photon Bioimaging. *Sci. Rep.* **2014**, *4*.

[43] Wang J.; Fang X.; Liang W. Pegylated Phospholipid Micelles Induce Endoplasmic Reticulum-Dependent Apoptosis of Cancer Cells but not Normal Cells. *ACS nano* **2012**, *6*, 5018–5030.

[44] IARC. *IARC Monographs on the Evaluation of the Carcinogenic Risk of Chemicals to Man*; World Health Organization: Lyon1999.

[45] Beddowes E. J.; Faux S. P.; Chipman J. K. Chloroform, carbon tetrachloride and glutathione depletion induce secondary genotoxicity in liver cells via oxidative stress. *Toxicology* **2003**, *187*, 101–115.

[46] Varkouhi A. K.; Scholte M.; Storm G.; Haisma H. J. Endosomal escape pathways for delivery of biologicals. *J. Control. Release* **2011**, *151*, 220–228.

[47] El-Sayed A.; Futaki S.; Harashima H. Delivery of macromolecules using arginine-rich cell-penetrating peptides: ways to overcome endosomal entrapment. *AAPS J.* **2009**, *11*, 13–22.

[48] Horth M.; Lambrecht B.; Khim M. C. L.; Bex F.; Thiriart C.; Ruysschaert J.-M.; Burny A.; Brasseur R. Theoretical and functional analysis of the SIV fusion peptide. *EMBO J.* **1991**, *10*, 2747–2755.

[49] Marsh M.; Helenius A. Virus Entry into Animal Cells. In *Advances in Virus Research* Maramorosch K, Murphy FA, Shatkin AJ, Eds.; Elsevier.1989; pp. 107–151.

[50] Felgner P. L.; Gadek T. R.; Holm M.; Roman R.; Chan H. W.; Wenz M.; Northrop J. P.; Ringold G. M.; Danielsen M. Lipofection: A highly efficient, lipid-mediated DNA-transfection procedure. *Proc. Nat. Acad. Sci. U.S.A.* **1987**, *84*, 7413–7417.

[51] Farhood H.; Serbina N.; Huang L. The role of dioleoyl phosphatidylethanolamine in cationic liposome mediated gene transfer. *Biochim. Biophys. Acta, Biomembr.* **1995**, *1235*, 289–295.

[52] Zhou X.; Huang L. DNA transfection mediated by cationic liposomes containing lipopolylysine: characterization and mechanism of action. *Biochim. Biophys. Acta, Biomembr.* **1994**, *1189*, 195–203.

[53] Nel A. E.; Madler L.; Velegol D.; Xia T.; Hoek E. M. V.; Somasundaran P.; Klaessig F.; Castranova V.; Thompson M. Understanding biophysicochemical interactions at the nano-bio interface. *Nat. Mater.* **2009**, *8*, 543–557.

[54] Boussif O.; LezoualC'H F.; Zanta M. A.; Mergny M. D.; Scherman D.; Demeneix B.; Behr J. P. A versatile vector for gene and oligonucleotide transfer into cells in culture and *in vivo*: Polyethylenimine. *Proc. Nat. Acad. Sci. U.S.A.* **1995**, *92*, 7297–7301.

[55] Pattrick N. G.; Richardson S. C. W.; Casolaro M.; Ferruti P.; Duncan R. Poly(amidoamine)-mediated intracytoplasmic delivery of ricin A-chain and gelonin. *J. Control. Release* **2001**, *77*, 225–232.

[56] Mellman I.; Fuchs R.; Helenius A. Acidification of the Endocytic and Exocytic Pathways. *Annu. Rev. Biochem.* **1986**, *55*, 663–700.

[57] Patil Y.; Panyam J. Polymeric nanoparticles for siRNA delivery and gene silencing. *Int. J. Pharm.* **2009**, *367*, 195–203.

[58] Thomas J. L.; Tirrell D. A. Polyelectrolyte-sensitized phospholipid vesicles. *Acc. Chem. Res.* **1992**, *25*, 336-342.

[59] Wickner W.; Schekman R. Membrane fusion. *Nat. Struct. Mol. Biol.* **2008**, *15*, 658–664.

[60] Hruban R. H.; Petersen G. M.; Ha P. K.; Kern S. E. Genetics of pancreatic cancer. From genes to families. *Surg. Oncol. Clin. N. Am.* **1998**, *7*, 1–23.

[61] Yamanaka Y.; Friess H.; Kobrin M. S.; Büchler M.; Kunz J.; Beger H. G.; Korc M. Overexpression of HER2/*neu* oncogene in human pancreatic carcinoma. *Hum. Pathol.* **1993**, *24*, 1127–1134.

[62] Goldstein A. M.; Fraser M. C.; Struewing J. P.; Hussussian C. J.; Ranade K.; Zametkin D. P.; Fontaine L. S.; Organic S. M.; Dracopoli N. C.; Clark Jr W. H. Increased risk of pancreatic cancer in melanoma-prone kindreds with p16 INK4 mutations. *New Engl. J. Med.* **1995**, *333*, 970–975.

[63] Pellegata N. S.; Sessa F.; Renault B.; Bonato M.; Leone B. E.; Solcia E.; Ranzani G. N. K-ras and p53 Gene Mutations in Pancreatic Cancer: Ductal and Nonductal Tumors Progress through Different Genetic Lesions. *Cancer Res.* **1994**, *54*, 1556–1560.

[64] Murphy K. M.; Brune K. A.; Griffin C.; Sollenberger J. E.; Petersen G. M.; Bansal R.; Hruban R. H.; Kern S. E. Evaluation of Candidate Genes MAP2K4, MADH4, ACVR1B, and BRCA2 in Familial Pancreatic Cancer: Deleterious BRCA2 Mutations in 17%. *Cancer Res.* **2002**, *62*, 3789–3793.

[65] Li D.; Xie K.; Wolff R.; Abbruzzese J. L. Pancreatic cancer. *Lancet* **2004**, *363*, 1049–1057.

[66] Almoguera C.; Shibata D.; Forrester K.; Martin J.; Arnheim N.; Perucho M. Most human carcinomas of the exocrine pancreas contain mutant cK-*ras* genes. *Cell* **1988**, *53*, 549–554.

[67] Lowy D.; Willumsen B. Function and regulation of ras. *Annu. Rev. Biochem.* **1993**, *62*, 851–891.

[68] Trahey M.; McCormick F. A cytoplasmic protein stimulates normal N-ras p21 GTPase, but does not affect oncogenic mutants. *Science* **1987**, *238*, 542–545.

[69] Arlt A.; Muerkoster S. S.; Schafer H. Targeting apoptosis pathways in pancreatic cancer. *Cancer Lett.* **2013**, *332*, 346–358.

[70] Takashima A.; Faller D. V. Targeting the RAS oncogene. *Expert Opin. Ther. Tar.* **2013**, *17*, 507–531.

[71] Tsuchida T.; Kijima H.; Hori S.; Oshika Y.; Tokunaga T.; Kawai K.; Yamazaki H.; Ueyama Y.; Scanlon K. J.; Tamaoki N.; Nakamura M. Adenovirus-mediated anti-K-ras ribozyme induces apoptosis and growth suppression of human pancreatic carcinoma. *Cancer Gene Ther.* **2000**, *7*, 373–383.

[72] Jasinski P.; Zwolak P.; Terai K.; Dudek A. Z. Novel Ras pathway inhibitor induces apoptosis and growth inhibition of K-ras-mutated cancer cells *in vitro* and *in vivo*. *Transl. Res.* **2008**, *152*, 203–212.

[73] Miura Y.; Ohnami S.; Yoshida K.; Ohashi M.; Nakano M.; Ohnami S.; Fukuhara M.; Yanagi K.; Matsushita A.; Uchida E.; Asaka M.; Yoshida T.; Aoki K. Intraperitoneal injection of adenovirus expressing antisense K-ras RNA suppresses peritoneal dissemination of hamster syngeneic pancreatic cancer without systemic toxicity. *Cancer Lett.* **2005**, *218*, 53–62.

[74] Brummelkamp T. R.; Bernards R.; Agami R. Stable suppression of tumorigenicity by virus-mediated RNA interference. *Cancer Cell* **2002**, *2*, 243–247.

[75] Yoshikawa K.; Tanabe E.; Shibata A.; Inoue S.; Kitayoshi M.; Okimoto S.; Fukushima N.; Tsujiuchi T. Involvement of oncogenic K-ras on cell migration stimulated by lysophosphatidic acid receptor-2 in pancreatic cancer cells. *Exp. Cell. Res.* **2013**, *319*, 105–112.

[76] Fleming J. B.; Shen G. L.; Holloway S. E.; Davis M.; Brekken R. A. Molecular consequences of silencing mutant K-ras in pancreatic cancer cells: Justification for K-ras-directed therapy. *Mol. Cancer Res.* **2005**, *3*, 413–423.